Mössbauer Effect Reference and Data Journal

September 2017 • Volume 40 • Number 7

Oxidation Reactions and Phonon Spectra in Catalysis Research

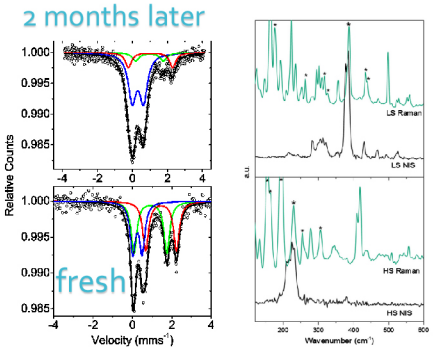

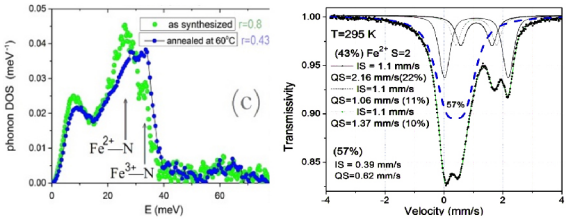

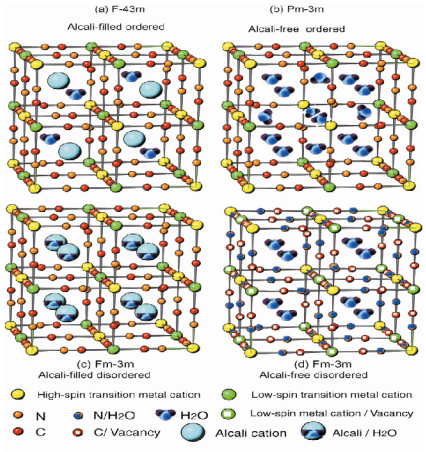

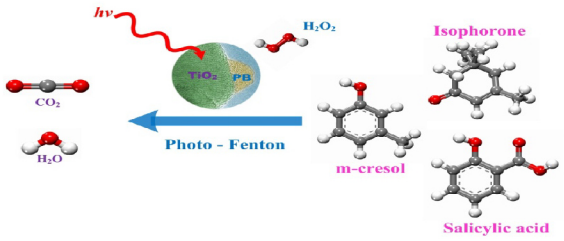

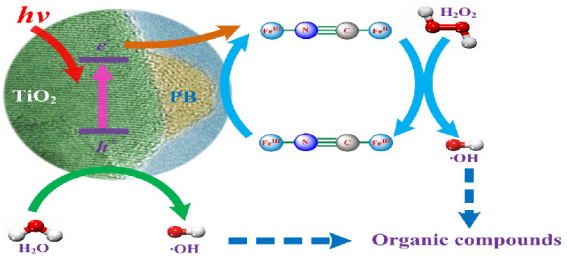

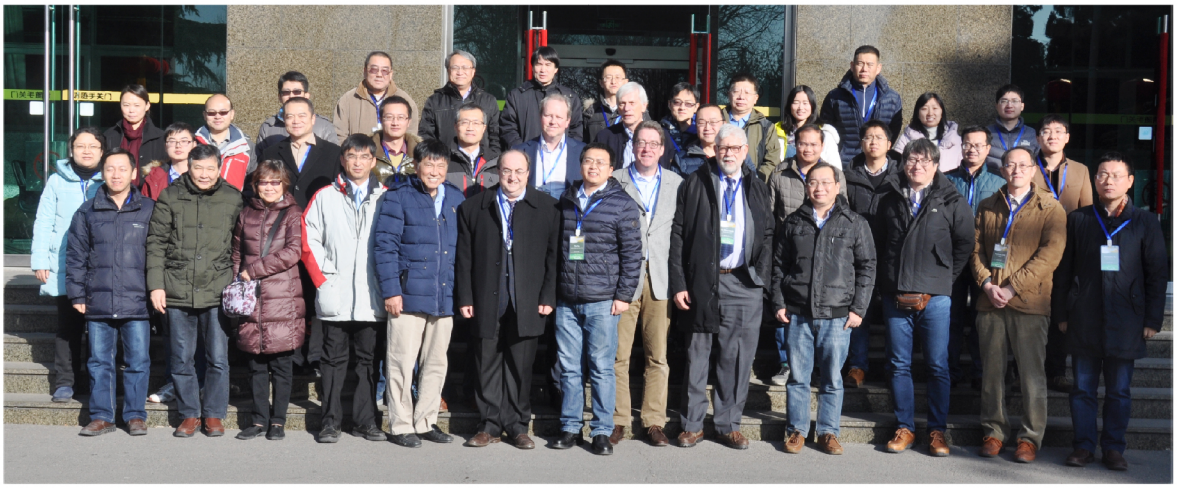

MÖSSBAUER SPECTROSCOPY
NEWSLETTER

September 2017

Oxidation Reactions and Phonon Spectra in Catalysis Research

A. I. Rykov[1], X. Li[1], W. Xu[2], D. Chen[2], J. Zhao[3], M. Y. Hu[3], W. Bi[3,4], T. S. Toellner[3], E. E. Alp[3], K. Nomura [5], R. Ge[1] and J. Wang[1]

[1]Mössbauer Effect Data Center, Dalian Institute of Chemical Physics, Chinese Academy of Sciences, Dalian 116023, China (Email: wangjh@dicp.ac.cn)

[2]Institute of High Energy Physics, Chinese Academy of Sciences, Beijing100049, China

[3]Advanced Photon Source, Argonne National Laboratory, Argonne, IL 60439, USA

[4]COMPRES, University of Illinois at Urbana Champaign, Urbana, Illinois, 61801

[5]Photocatalysis International Research Center, Tokyo University of Science, Yamazaki, Noda, Chiba 278-8510, Japan

Attractive methods to explore the solid phase transformations in the course of catalytic reactions are the straight and phonon-assisted Mössbauer spectroscopies. Quite simultaneous implementation of these techniques realizable now with the 3rd generation synchrotron facilities permits tracking the coherent changes in the Fe-projected vibrations, valences, environments, crystal fields, and spin densities on Fe along the chemical conversion processes [1].

In soft matter catalysts, non-Debye behavior manifest itself in the vibrational density of states as an excess of low-energy vibrational excitations over the level of Debye model. This is the common feature of soft matter including polymer frameworks, colloids, granular nanomaterials, liquid crystals, nanocomposites and biological materials.

Among them are the double-metal cyanides (DMC), which offer appealing perspectives as molecular sieves, cation exchangers, and electron scavengers useful in a wide family of catalytic reactions. Mixed valence of some of the 3*d* metals is an important functional property of these catalysts responsible for the maintenance and regeneration of the catalytic activity. In the course of a catalytic operation, the catalyst intervenes in redox reactions, which affect the oxidation state of the embedded 3*d* metal ions. Initially, the oxidation and reduction proceed with different rates, so that the average valence of a 3*d* metal changes towards an equilibrium value. In this initial step of the catalyst functioning, the overall composition is changing, and the catalytic activity could decrease, however, the catalyst is not degrading in the sense of contamination or poisoning-related degradation. As the composition of the catalyst reaches the equilibrium composition, the compound becomes functioning as a true catalyst, whose phase composition remains invariant [2, 3].

In this work, we are focusing on the catalyst whose composition varies between the ferric and ferrous hexacyanocobaltates. The DMC's $Fe[Co(CN)_6]\cdot 2H_2O$ [4] and $Fe_3[Co(CN)_6]_2\cdot 12H_2O$ [5] are two end-members of a series of solid solutions, whose density decreases with increasing the water content. Mixed valence composition is related to Mössbauer subspectra area ratio $r = A(Fe^{2+})/A(\text{total})$. In some approximation, r is close to the ratio of valence concentrations $[Fe^{2+}]/([Fe^{3+}]+[Fe^{2+}])$. The solid solutions with r of 0.9 or 0.99 are ordinarily synthesized when one attempts to synthesize $Fe_3[Co(CN)_6]_2\cdot 12H_2O$. This is probably the result of unsolicited oxidation at synthesis. The r value can be easily identified with Mössbauer spectroscopy owing to the spectral asymmetry which increases with increasing r (see the spectra in Refs.[6, 7]). It is the pivotal role of Mössbauer spectroscopy in the studies of DMC's [8, 9] that permits us to notice the deviation of r from 1 at the level of a few percent.

The above mentioned solid solutions were shown to be efficient sorbents for removal of Cs^+[6], and photo-Fenton oxidation catalysts

[6, 7, 10], in particular, for the oxidation of bisphenol A [10]. The value of r drops by an order of magnitude from the initial value of 0.89 to 0.08 as the catalyst densifies in the course of the photo-Fenton reaction [7]. Thus, the catalyst compound, which is initially close to one end, evolves under usage towards another end member of the solid solution. The smallness of the difference between the lattice parameters of $Fe[Co(CN)_6]\bullet 2H_2O$ (a = 1.018 nm) and $Fe_3[Co(CN)_6]_2\bullet 12H_2O$ (a = 1.028 nm) makes difficult detection of a possible miscibility gap between these end-member compounds.

Another complication arises starting part way through the catalyst exploitation. Not only the valence of iron changes within the main phase, but also an admixture of second phase must appear because of the differentFe:Co stoichiometry for the initial and spent catalyst. The nano-sized second-phase precipitates were observed indeed after the reaction. It is difficult to identify the nanophase in the XRD patterns, however, FT-IR spectra exhibit an adsorption band from a "Fe-O" phase at 590 cm^{-1} [7].

In this work, we report on the change of the Fe-projected vibrational spectrum as the content of Fe^{3+} increases at the expense of decreasing content of Fe^{2+}. In place of photo-Fenton oxidation, we applied the slow oxidation annealing in mild conditions (air, moderate temperature of 60 °C).

Figure 1(a) shows initially the weight loss associated with the dehydration, which is overbalanced at times longer than 300 min by the weight gain associated with the oxidation. No increase of weight was observed in thermogravimetric curve when the sample chamber was filled with Ar atmosphere.

The enriched starting material $^{57}Fe[Co(CN)_6]_{0.73}$ was synthesized using $^{57}Fe_2O_3$ dissolved in hydrochloric acid solution; the acidic medium has led to somewhat low r = 0.8. Upon air-oxidation at 60 °C the valence ratio decreased to r = 0.43 as detected by Mössbauer spectroscopy as shown in Figure 1(b). The spectra showed similar changes upon the Fenton and air-annealed treatments, except that latter process gave the incomplete oxidation (r = 0.43), suggesting that the miscibility gap probably does not exist.

The residual contribution of Fe^{2+} can be resolved into three doublets similarly to the spectra of the as-synthesized sample [11]. Also, parameters of isomer shift and quadrupole splitting of Fe^{2+} remain quite similar to those in both initial and spent

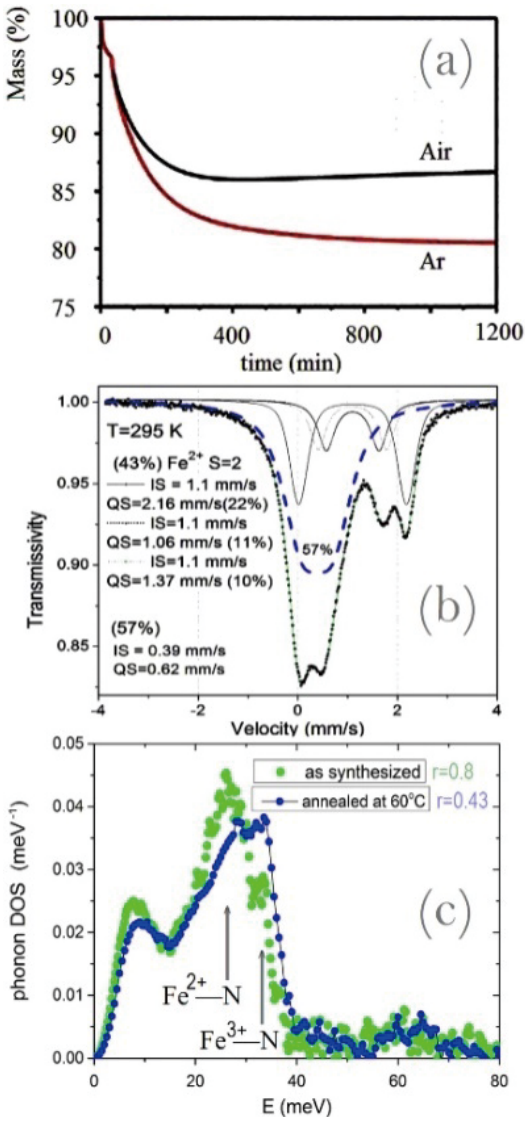

Figure 1. Dehydration curve of the as-synthesized sample in air (a), ^{57}Fe Mössbauer spectrum of the air-annealed sample (b), and the phonon density of states in the as-synthesized and air-annealed samples (c). The percentage in (b) shows the areas of $A(Fe^{2+})/A$(total) and $A(Fe^{3+})/A$(total).

catalyst used in the photo-Fenton catalysis studies [7, 10]. As to the question of why there exist in ferrous hexacyanocobaltates(III) and hexacyanochromates(III) many different Fe^{2+} sites, which was a puzzle for years, controversial answers can be found in early literature [12-14]. Previous assignments of some of Fe^{2+} to an "interstitial Fe" site [12, 13] were inconsistent with the model of occupational disorder among the species represented by the 1nm-wide void and the whole complex $Co(CN)_6$(or $Cr(CN)_6$), as given by Ludi and Güdel [15]. It was understood

later [14] that the Ludi model implied the existence of several ligand conformations around Fe^{2+}. In accordance with the reported structure [5, 15], the comprehensive assignments of the Mössbauer doublets to a variety of ligand conformations around Fe^{2+} was given recently [6, 11, 16].

It is worth to note that the area ratio r does not give the exact value of the Fe^{2+} fraction, but its lower bound, because the Fe-O phase contributes to the Fe^{3+} spectral area with the enhanced Lamb-Mössbauer factor f_{LM}. In the room-temperature spectra of many oxides, evaluated previously by De Grave and Van Alboom [17], taking simply the area ratio overestimates typically the value of $[Fe^{2+}]/[Fe^{3+}]$ with an error of 15% on average.This estimate is relevant to the case when both Fe^{2+} and Fe^{3+} are enclosed into the same phase, in which Fe^{3+} is bound more tightly owing to its higher charge. The same estimate was confirmed by McCammon in perovskite [18], the structural prototype of the Prussian blue analogs (PBA). In the dense and void-diluted end-member PBA's, $Fe[Co(CN)_6]\bullet 2H_2O$ and $Fe_3[Co(CN)_6]_2\bullet 12H_2O$, Fe^{3+} is bound by 6 charged (CN^-) ligands, whereas Fe^{2+} is bound, on average, by 4 charged and 2 neutral (H_2O) ligands.

In the spent catalyst, or in air-annealed sample, another fraction of Fe^{3+} exists bound within the oxide/hydroxide phase.The oxygen is supplied and the "Fe-O" nanophase [7] is crystallized only at the surface of a DMC particle, therefore, the reaction must be limited by the surface diffusion of iron towards the nuclei of the new phase. While the reaction is incomplete, one can suggest a plausible equation for the complete reaction:

$$10Fe_3[Co(CN)_6]_2\bullet 12H_2O + 7.5O_2 = 20Fe[Co(CN)_6]\bullet 2H_2O + Fe_{10}O_{14}(OH)_2 + 9H_2O \quad (1)$$

The second "Fe-O" phase [7] is expressed as the ferrihydrite $Fe_{10}O_{14}(OH)_2$, the nanocrystalline material [19], which form no crystals larger than a few nm. This is a typical impurity in DMC [20]. The ferrihydrite is also a plausible candidate for the second phase precipitates because the value of quadrupole splitting in ferrihydrite is consistent with the observed parameters, shown in our Figure 1(b).

There arises a question of why the oxidation reaction is incomplete even after such a long oxidative treatment? The main phase on the right hand in Eq. (1) contains no voids of $Co(CN)_6$, therefore, the surface of powder shrinks as shagreen as every third of Fe ions diffuses towards the precipitates. Densification of the structure inhibits the surface diffusion of iron, so that the reaction is arrested at a significant residual concentration of Fe^{2+}.

Assuming that the as-synthesized sample consists of a single phase containing some concentrations $[Fe^{2+}]$ and $[Fe^{3+}]$ and taking into account De Grave's coefficient 1.15 for a better visibility of Fe^{3+} the area ratio r can be expressed as

$$r = 0.8 = \frac{[Fe^{2+}]}{1.15[Fe^{3+}]+[Fe^{2+}]} \quad (2)$$

At this stage, we estimate the true concentrations $[Fe^{2+}]$ of 82% and $[Fe^{3+}]$ of 18%. The correction of 2% reflects our expectation of a slightly higher factor f_{LM} in the dense $Fe[Co(CN)_6]\bullet 2H_2O$ compared to the void-diluted $Fe_3[Co(CN)_6]_2\bullet 12H_2O$. The Debye temperature in alkali-free Prussian blue and its analogs is known to vary in the range between 180 K and 257 K [21-23]. On the other hand, the Debye temperatures estimated in the ferrihydrite is about 500 K [24]. Therefore, the visibility of Fe^{3+} would increase further as far as the catalyst oxidation proceeds, because for the ferrihydrite the $f_{LM}(300K)$ is twice higher than for PBA. The doubling factor of 2 would be in order to account for the increased visibility of Fe^{3+} in ferrihydrite. According to the Eq. (1), when a concentration C of Fe^{2+} enters the oxidation process, then $C/3$ Fe^{3+} is added to the ferrihydrite and $2C/3$ Fe^{3+} is added to the main phase. In the sample annealed in air at 60 °C,

$$r = 0.43 = \frac{[0.82-C]}{1.15[0.18]+[0.82-C]+1.15[2\frac{C}{3}]+2[\frac{C}{3}]}. \quad (3)$$

This solves to the conversion rate C = 0.32, and the true concentrations of 50% are thus found for each of $[Fe^{2+}]$ and $[Fe^{3+}]$. The coefficients beyond the square brackets in Eq. (3) are shown for T = 300 K, however, a generalization of the Eq. (3) with temperature-dependent coefficients will describe the effect of unmasking Fe^{3+} with increasing temperature. The apparent contribution of Fe^{3+} into the spectral area increases with temperature both in main phase and in Fe-O phase. When the admixture of Fe^{3+} is small,the unmasking effect will produce the temperature-dependent asymmetry. Nature of this asymmetry was a subject of previous investigation [25]. Here, we suggest the origin of the asymmetry different than the one proposed in Ref. [25].

The Fe phonon density of states derived from the spectra of nuclear inelastic scattering (NIS) confirms further the bond strengthening for Fe^{3+} compared to Fe^{2+}. The vibrational density of states (DOS) exhibits the peaks at 26 and 34 meV, the latter increasing under oxidation at the expense of the former as shown in Figure 1(c). The frequency hardening by 30% is related to the increase in the bond stiffness by 15%. These DOS peaks are assigned to the Fe^{2+}-N and Fe^{3+}-N stretching vibrations, respectively. This is a typical change associated with the charge transfer in PBA. In the external sphere of the ferricyanide complex, the similar stretching vibrations were identified previously at 220 and 280 cm^{-1} [26].

The precipitates of the second phase are expected to produce some peak at a lower energy. For example, in iron oxides, Nomura et al [27] have published the iron-projected phonon densities of states peaked near 20 meV. In this region, we observe the DOS nearly unchanged, although the contribution of the main phase decreases as the overall content of iron in the main phase decreases. This is most probably due to the contribution of the ferrihydrite precipitates.

The interesting change takes place also in the low-energy part of the DOS. A close inspection of the low-energy peak fitted with a sigmoidal function to smooth the noise is the subject of Figure 2, which reveals the shift of the peak maximum from 8 meV to 9 meV. The broad peak represents a bunch of modes, one of which is shown by inset in Figure 2. This is an optical mode, characterized by the rotation of the octahedric rigid units. The rigid unit modes (RUMs) are optic modes, however, they are located at such low energies, where they must be mixing into the band of transverse acoustic modes, which occupy the broad regions outside of the center of Brillouin zone to form Van Hove singularities near its edges. The hybridized transverse modes manifest themselves in the inelastic neutron scattering [28, 29] and give rise to the negative thermal expansion (NTE) [4, 30]. In the end members of our series the NTE was observed at the level of -1.5 ppm per K for $Fe[Co(CN)_6]\cdot 2H_2O$ [4], and -4.0 ppm per K for $Fe_3[Co(CN)_6]_2\cdot 12H_2O$ [30]. Large NTE coefficients are frequently associated with the transverse mode peaks at very low energies, in such a way that the softer is the mode energy the larger is the absolute value of the NTE coefficient [28]. We observe indeed in Figure 2 that the peak hardens as we go from NTE of -4 ppm per K towards NTE of -1.5 ppm per K.

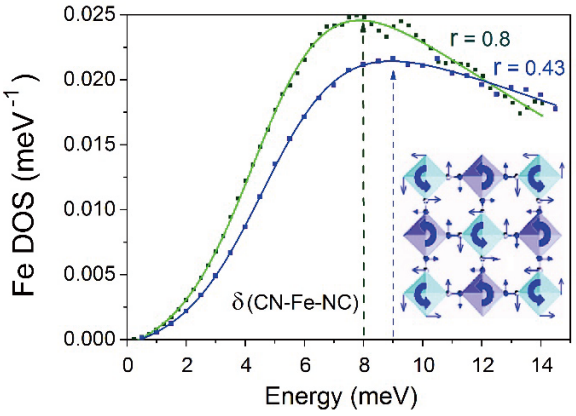

Figure 2. The low-energy region of the phonon DOS in the two samples with theMössbauer area ratio r = A(Fe^{2+})/A(total) of 0.8 and 0.43. The inset shows one of the rigid-unit-modes (RUM's) involving the FeN_6 and CoC_6 octahedra as rigid units. The low-energy DOS peak is assigned to the Van Hove singularity of transverse acoustic modes at Brillouin zone hybridized with the RUMs.

The Lamb-Mössbauer factor f_{LM} is mostly determined by the low-energy region of DOS, wherein the peak shift is observed. This can be seen from the expression [31] for the temperature dependence of f_{LM}:

$$f_{LM}(T) = \exp\left(-E_R\int_0^{\infty}\frac{g(E)}{E}\coth\left(\frac{E}{2k_BT}\right)dE\right) \quad (4)$$

The function f_{LM}(T) is expressed through the phonon density of states g(E), the phonon energy E, the Boltzmann's constant kB and temperature T. The recoil energy E_R received by a free atom with mass M is defined by the energy conservation law, $E_R = E_\gamma / 2Mc^2$($E_R \approx$ 2meV for ^{57}Fe). Here E_γ is the energy of γ-radiation and c is the light velocity.For the energies below 50 meVat T = 290 K the rigorous Eq. (4) can be simplified with high accuracy (better than 1%) using the Taylor expansion:

$$\coth(x) = x^{-1}+x/3+O(x^3) \quad (4)$$

Then, the integration term can be represented by

$$\frac{g(E)}{E^2}2k_BT + \frac{1}{6k_BT} \quad (5)$$

Or, substituting 50 meV for $2k_BT$, we have under the integration the expression

$$50\frac{g(E)}{E^2} + \frac{1}{150} \quad (6)$$

This derivation is made to show that the origin of above mentioned De Grave's correction with the factor of 1.15 can be readily observed via the comparison ofthe areas under the E^{-2} weighted DOS $g(E)/E^2$. In the DOS of the as-synthesized sample, the low-energy peak is stronger. Moreover, because it is located at the lower energy of 8 meV, we observe in Figure 3 this peak even more enhanced with the weighting factor of E^{-2}. The area under the weighted DOS $g(E)/E^2$ decreases indeed by about 15%. The important finding of this work is that the main change in the area (shaded) takes place in the low-energy region. Thus, the increase in bond stiffness for the Fe^{3+} compared to Fe^{2+} suppress the lowest-energy part of the transverse modes associated with the rotational motion of the RUMs. To put it in broader terms, the recoilless fraction increases at the expense of the arrested softest modes.

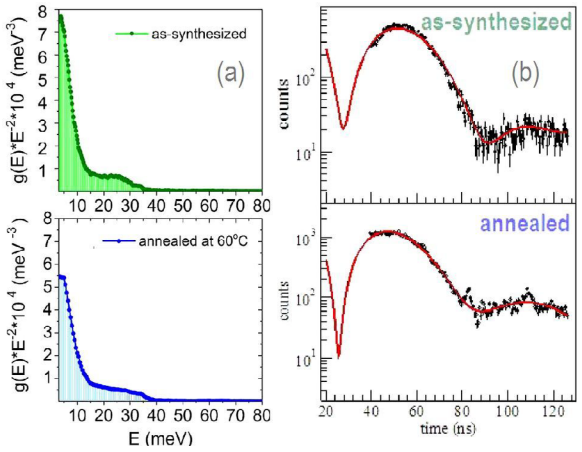

Figure 3. E^{-2}-weigthed DOS (a) and nuclear forward scattering (b) in the two samples of Fe.

Finally, the Figure 3(b) shows the result of the time-domain Mössbauer spectroscopy applied to both samples. Fourrier transformation of the time-domain spectra to the energy domain is capable to ensure a better spectral resolution (narrower linewidth [32]) than that in the conventional Mössbauer spectra. This is because the synchrotron experiment obviates the resolution limitation associated with the source natural linewidths. To improve the resolution one has to run the synchrotron in the bunch regime allowing the measurement of the time-domain spectra in wider time window, such as 500 ns [32]. Nevertheless, we could observe in Figure 3(b) as many as two cycles of quantum beat pattern. The quantum beatings decrease in amplitude as we proceed from more or less symmetric to asymmetric conventional Mössbauer spectra. This is quite expected result since in the limit of fully asymmetric doublet we obtain a single line, which produces no quantum beats at all.

In this work, we applied the vibrational spectroscopy to investigate the changes of a Prussian Blue analogue in the course of reaction associated with the charge transfer. Owing to the seemingly simple structure, various properties of PBA could be recently predicted by the density functional theory. However, it is hard to expect the DFT predicting the singularity observed in $g(E)/E^2$ at E approaching to zero. The behavior of the low-energy excitation in this region deviates clearly from Debye-like [33]. Separation of vibrational and quasielastic excitations in such "soft-matter" systems is not obvious procedure. Diffusion of water molecules, related to proton conductivity, and discrete rotations of CN-ligands, associated with long-living tautomers, may contribute to quasi-elastic scattering quite near the elastic peak associated with the low-energy motions of Fe.The strain-exchange between the Fe and Co metal centers is probably not simply the interaction by the field of plane waves. The phonon spectra bearing the non-Debye character in the low-energy region are supposedly a prerequisite for unusual behaviors, related to intriguing applications of these compounds.

This work was financially supported by the Chinese Academy of Sciences Visiting Professorships for Senior International Scientists (2011T1G15) and the National Natural Science Foundation of China (21476232).

REFERENCES

[1] K. Liu, A. I. Rykov, J. Wang, and T. Zhang, "Chapter One-Recent Advances in the Application of Mößbauer Spectroscopy in Heterogeneous Catalysis," *Advances in Catalysis*, vol. 58, pp. 1-142, 2015.

[2] V. Parmon, A. Emeline, and N. Serpone, "Glossary of terms in photocatalysis and radiocatalysis," *Int. J. Photoenergy*, vol. 4, pp. 91-131, 2002.

[3] D. Kolb, "Catalysis," *J. Chem. Educ*, vol. 56, no. 11, p. 743, 1979.

[4] S. Margadonna, K. Prassides, and A. N. Fitch, "Zero thermal expansion in a Prussian blue analogue," *Journal of the American Chemical Society*, vol. 126, no. 47, pp. 15390-15391, 2004.

[5] D. Mullica, J. Oliver, W. Milligan, and F. Hills, "Ferrous hexacyanocobaltate dodecahydrate," *Inorganic and Nuclear Chemistry Letters*, vol. 15, no. 9-10, pp. 361-365, 1979.

[6] A. I. Rykov, J. Wang, T. Zhang, and K.

Nomura, "Cs sorption by “soluble” and “insoluble” iron hexacyanocobaltates probed by Mössbauer spectroscopy," *Hyperfine Interactions*, vol. 218, no. 1-3, pp. 53-58, 2013.

[7] X. Li *et al.*, "Excellent photo-Fenton catalysts of Fe–Co Prussian blue analogues and their reaction mechanism study," *Applied Catalysis B: Environmental*, vol. 179, pp. 196-205, 2015.

[8] F. Grandjean, G. J. Long, and L. Samain, "The Pivotal Role of Mössbauer Spectroscopy in the Characterization of Prussian Blue and Related Iron Cyanide Complexes," *Mössbauer Effect Reference and Data Journa*l, vol. 35, no. 6, pp. 144-155, 2012.

[9] X. Li *et al.*, "Prussian blue/TiO_2 nanocomposites as a heterogeneous photo-Fenton catalyst for degradation of organic pollutants in water," *Catalysis Science & Technology*, vol. 5, no. 1, pp. 504-514, 2015.

[10] X. Li, A. I. Rykov, and J. Wang, "Hydrazine drastically promoted Fenton oxidation of bisphenol A catalysed by a Fe^{III}–Co Prussian blue analogue," *Catalysis Communications*, vol. 77, pp. 32-36, 2016.

[11] A. Rykov, J. Wang, T. Zhang, and K. Nomura, "Mixed Orbital Ground States of Fe^{2+} in Prussian Blues," *arXiv preprint arXiv:1302.2192*, 2013.

[12] D. B. Brown, D. F. Shriver, and L. H. Schwartz, "Solid-state reactions of iron(II) hexacyanochromate(III)," *Inorganic Chemistry*, vol. 7, no. 1, pp. 77-83, 1968.

[13] K. Maer Jr, M. Beasley, R. Collins, and W. Milligan, "Structure of the titanium-iron cyanide complexes," *Journal of the American Chemical Society*, vol. 90, no. 12, pp. 3201-3208, 1968.

[14] P. G. Rasmussen and E. Meyers, "An investigation of Prussian blue analogues by Mössbauer spectroscopy and magnetic susceptibility," *Polyhedron*, vol. 3, no. 2, pp. 183-190, 1984.

[15] A. Ludi and H. U. Güdel, "Structural chemistry of polynuclear transition metal cyanides," in *Inorganic Chemistry*: Springer, 1973, pp. 1-21.

[16] A. I. Rykov, X. Li, and J. Wang, "Crystal structure refinement of the electron-transfer-active potassium manganese hexacyanoferrates and isomorphous potassium manganese hexacyanocobaltates," *Journal of Solid State Chemistry*, vol. 227, pp. 35-44, 2015.

[17] E. De Grave and A. Van Alboom, "Evaluation of ferrous and ferric Mössbauer fractions," *Physics and chemistry of minerals*, vol. 18, no. 5, pp. 337-342, 1991.

[18] C. McCammon, "The crystal chemistry of ferric iron in $Fe_{0.05}Mg_{0.95}SiO_3$ perovskite as determined by Mössbauer spectroscopy in the temperature range 80–293 K," *Physics and Chemistry of Minerals*, vol. 25, no. 4, pp. 292-300, 1998.

[19] F. M. Michel *et al.*, "The structure of ferrihydrite, a nanocrystalline material," *Science*, vol. 316, no. 5832, pp. 1726-1729, 2007.

[20] C. Gervais, M.-A. Languille, G. Moretti, and S. Reguer, "X-ray photochemistry of Prussian blue cellulosic materials: Evidence for a substrate-mediated redox process," *Langmuir*, vol. 31, no. 29, pp. 8168-8175, 2015.

[21] J. Fenger and J. Olsen, "Temperature-dependent after-effects of the cobalt-57–iron-57 electron-capture reaction in $Cd_3[^{57}Co(CN)_6]_2$ $12H_2O$," *Journal of the Chemical Society, Dalton Transactions*, no. 3, pp. 319-323, 1974.

[22] P. Zhou, D. Xue, H. Luo, and H. Shi, "Temperature dependence of the Mössbauer effect on prussian blue nanowires," *Hyperfine interactions*, vol. 141, no. 3-4, pp. 601-606, 2002.

[23] G. Félix *et al.*, "Enhanced Cooperative Interactions at the Nanoscale in Spin-Crossover Materials with a First-Order Phase Transition," *Physical Review Letters*, vol. 110, no. 23, p. 235701, 2013.

[24] S. Dubiel, J. Cieślak, I. Alenkina, M. Oshtrakh, and V. Semionkin, "Evaluation of the Debye temperature for iron cores in human liver ferritin and its pharmaceutical analogue, Ferrum Lek, using Mössbauer spectroscopy," *Journal of Inorganic Biochemistry*, vol. 140, pp. 89-93, 2014.

[25] E. Reguera, H. Yee-Madeira, S. Demeshko, G. Eckold, and J. Jimenez-Gallegos, "Nature of the Observed Asymmetry in Mössbauer Spectra of Iron(2+) Hexacyanometallates(III)," *Zeitschrift für Physikalische Chemie International journal of research in physical chemistry and chemical physics*, vol. 223, no. 6, pp. 701-711, 2009.

[26] J. Lejeune, J.-B. Brubach, P. Roy, and A. Bleuzen, "Application of the infrared spectroscopy to the structural study of Prussian blue analogues," *Comptes Rendus Chimie*, vol. 17, no. 6, pp. 534-540, 2014.

[27] K. Nomura *et al.*, "Mössbauer and vibrational DOS studies of diluted magnetic tin oxides and nano iron oxides," *Hyperfine Interactions*, vol. 224, no. 1-3, pp. 25-33, 2014.

[28] K. W. Chapman, M. Hagen, C. J. Kepert, and P. Manuel, "Low energy phonons in the NTE compounds $Zn(CN)_2$ and $ZnPt(CN)_6$," *Physica B: Condensed Matter*, vol. 385, pp. 60-62, 2006.

[29] S. Adak, L. L. Daemen, and H. Nakotte, "Negative thermal expansion in the Prussian Blue analog $Zn_3[Fe(CN)_6]_2$: X-ray diffraction and neutron vibrational studies," *Journal of Physics: Conference Series*, vol. 251, p. 012007, 2010.

[30] S. Adak, L. L. Daemen, M. Hartl, D. Williams, J. Summerhill, and H. Nakotte, "Thermal expansion in 3*d*-metal Prussian Blue Analogs—A survey study," *Journal of Solid State Chemistry*, vol. 184, no. 11, pp. 2854-2861, 2011.

[31] W. Sturhahn and A. Chumakov, "Lamb–Mössbauer factor and second-order Doppler shift from inelastic nuclear resonant absorption," *Hyperfine Interactions*, vol. 123, no. 1-4, pp. 809-824, 1999.

[32] A. Rykov, K. Nomura, and J. Wang, "Fourier spectra of resonant nuclear forward scattering: lineshape dependence on absorber thickness distribution," *Hyperfine Interactions*, vol. 222, no. 1, pp. 45-55, 2013.

[33] A. I. Rykov, K. Nomura, T. Mitsui, and M. Seto, "Low-energy excitations in brownmillerites and related oxides," *Physica B: Condensed Matter*, vol. 350, no. 4, pp. 287-304, 2004.

P1

Oxidation Reactions and Phonon Spectra of Fe-Co PBA

A. I. Rykov[1], X. Li[1], W. Xu[2], D. Chen[2], J. Zhao[3], M. Y. Hu[3], W. Bi[3,4], T. S. Toellner[3], E. E. Alp[3], Nomura K[5], R. Ge[1] and J. Wang[1]

[1]Mössbauer Effect Data Center, Dalian Institute of Chemical Physics, Chinese Academy of Sciences, Dalian 116023, China

[2]Institute of High Energy Physics, Chinese Academy of Sciences, Beijing 100049, China

[3]Advanced Photon Source, Argonne National Laboratory, Argonne, IL 60439, USA

[4]COMPRES, University of Illinois at Urbana Champaign, Urbana, Illinois, 61801

[5]Photocatalysis International Research Center, Tokyo University of Science, Yamazaki, Noda, Ciba 278-8510, Japan

P2

Conventional and Phonon-assisted Mössbauer Spectroscopies Application to Chemical Transformations

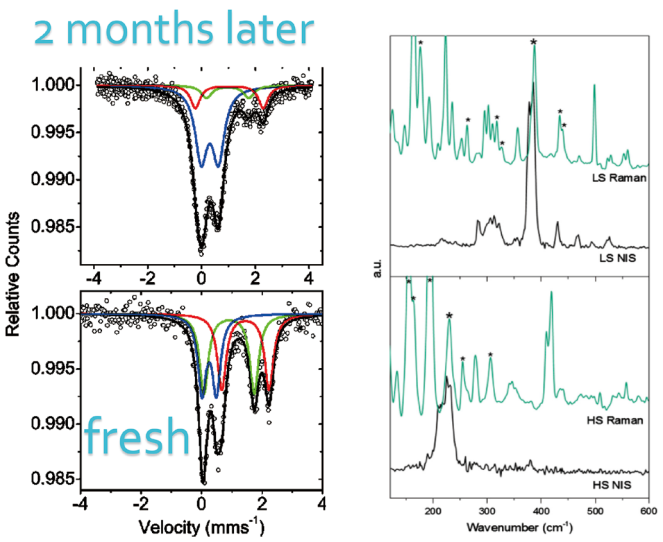

P3

Double-Metal Cyanides as Mixed-Valence Compounds and Their Behavior in Catalytic Reactions

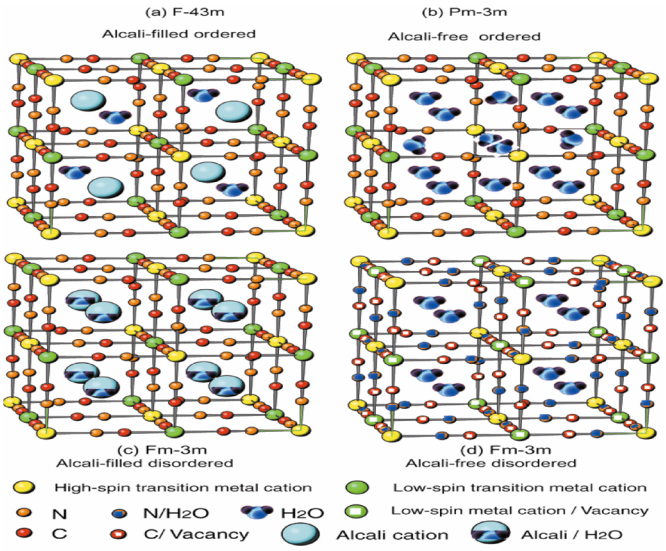

P4

The DMC Intermediate between $Fe[Co(CN)_6]\cdot 2H_2O$ and $Fe_3[Co(CN)_6]_2\cdot 12H_2O$

Ferric hexacyanocobaltates(III): $Fe[Co(CN)_6]\cdot 2H_2O$

Ferrous hexacyanocobaltates(III): $Fe_3[Co(CN)_6]_2\cdot 12H_2O$

Mössbauer subspectra area ratio r = $A(Fe^{II})/A(total)$. In some approximation, r is close to the ratio of valence concentrations $[Fe^{II}]/([Fe^{III}] + [Fe^{II}])$.

The solid solutions with r of 0.9 or 0.99 are ordinarily synthesized when one attempts to synthesize $Fe_3[Co(CN)_6]_2\cdot 12H_2O$.

It is the pivotal role of Mössbauer spectroscopy in the studies of DMC's that permits us to notice the deviation of r from 1 at the level of a few percent.

P5

Examples of the Catalytic Reactions Using DMC , in Particular, Reaction in which the Composition of a Catalyst Changes

Photon-Fenton Reaction

$Fe^{2+} + H_2O_2 \rightarrow Fe^{3+} + {\bullet}OH + OH^-$ $k_1 = 76\ M^{-1}S^{-1}$

$Fe^{3+} + H_2O_2 \rightarrow Fe^{2+} + HO_2{\bullet} + H^+$ $k_2 = 0.02\ M^{-1}S^{-1}$

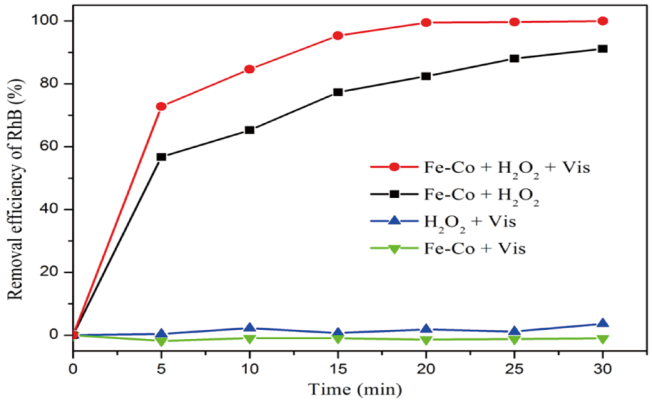

P6

^{57}Fe Mössbauer Spectra of Fe^{II}-Co PBA (a) before, (c) after; Fe^{III}-Co PBA (b) before, and (d) after Photo-Fenton Reactions.

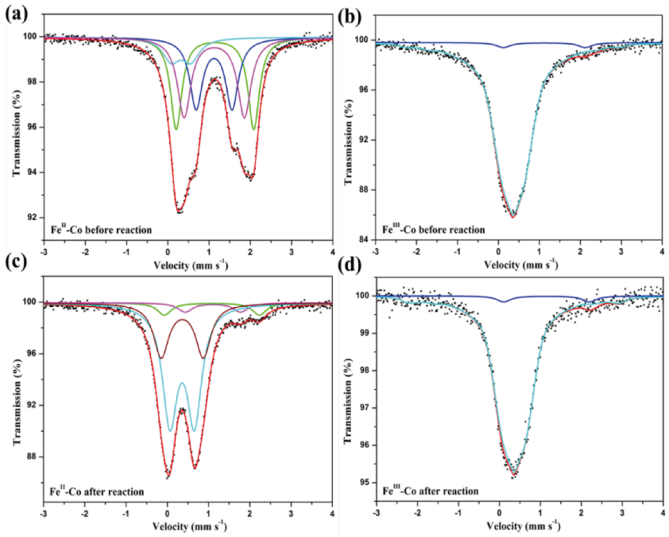

P7

Formation of a Second Phase in the Course of a Catalytic Reaction

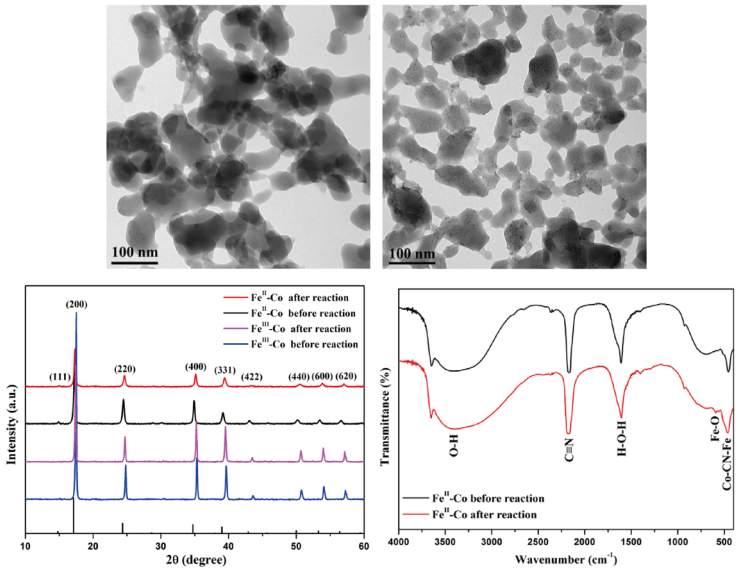

P8

Similar Oxidation Process Occurrence at Annealing in Mild Conditions

Today, we report on the change of the ^{57}Fe-projected vibrational spectrum of Fe^{II}-Co PBA as the content of Fe^{III} increases at the expense of decreasing content of Fe^{II}. In place of photo-Fenton oxidation, we applied the slow oxidation at annealing in mild conditions (air, moderate temperature of 60 ^{o}C).

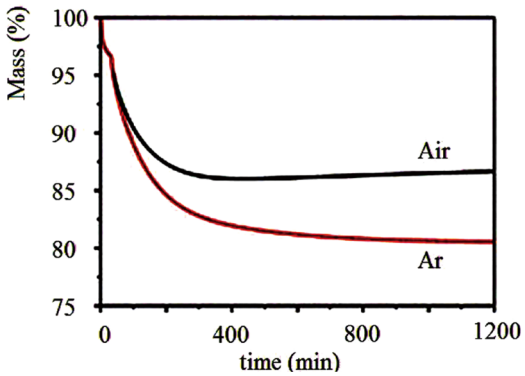

P9

Conventional ^{57}Fe Mössbauer Spectra after the Oxidation

The enriched starting material $^{57}Fe_3[Co(CN)_6]_2 \cdot 12H_2O$ was synthesized using $^{57}Fe_2O_3$ in hydrochloric acid solution; the acidic medium has led to somewhat low r = 0.8. Upon air-oxidation at 60 ^{o}C the valence ratio decreased to r = 0.43 as detected by Mössbauer spectra.

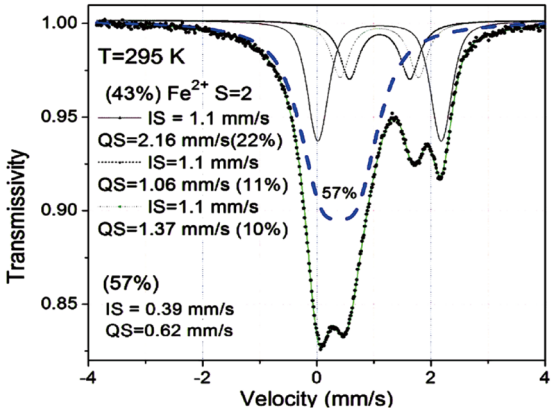

P10

Interpretation of the Multiple Fe^{II} Subspectra

Component	Assignment		IS (mm s^{-1})	QS (mm s^{-1})	2Γ (mm s^{-1})	Area (%)
$Fe_3[Co(CN)_6]_2$	Fe^{III}	6N	0.32(1)	0.48(3)	0.51(5)	20
	Fe^{II}	1/2Trans(H_2O) & 5/4N	1.122(3)	0.871(9)	0.37(1)	23
		3Fac(H_2O) & 3N	1.125(2)	1.46(1)	0.39(2)	22
		2Cis/3Mer(H_2O) & 4/3N	1.143(2)	1.881(9)	0.33(1)	35
$Fe_3[Co(CN)_6]_2$ after	Fe^{III}	6N	0.32(1)	0.48(3)	0.51(5)	57
	Fe^{II}	1/2Trans(H_2O) & 5/4N	1.122(3)	0.871(9)	0.37(1)	11
		3Fac(H_2O) & 3N	1.125(2)	1.46(1)	0.39(2)	10
		2Cis/3Mer(H_2O) & 4/3N	1.143(2)	1.881(9)	0.33(1)	22

P11

Balancing Chemical Equation for the Oxidation of the DMC

- While the reaction is incomplete, one can suggest a plausible equation for the complete reaction:

$$10Fe_3[Co(CN)_6]_2 \cdot 12H_2O + 7.5O_2 = 20Fe[Co(CN)_6] \cdot 2H_2O + Fe_{10}O_{14}(OH)_2 + 9H_2O$$

- The second "Fe-O" phase is expressed as the ferrihydrite $Fe_{10}O_{14}(OH)_2$.

P12

Reasons for Arresting the Oxidation Reaction

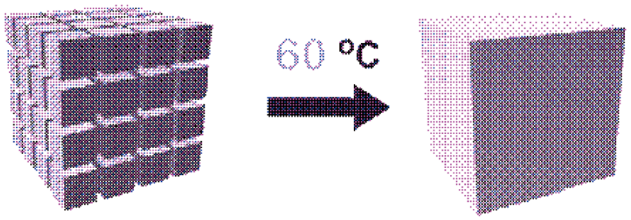

Densifying the PBA through oxidation

Reduction of the specific surface at the densification process from $Fe_3[Co(CN)_6]_2 \cdot 12H_2O$ to $Fe[Co(CN)_6] \cdot 2H_2O$

P13

Change of ^{57}Fe Projected Vibrational Density of States upon Oxidation in Air at 60 °C

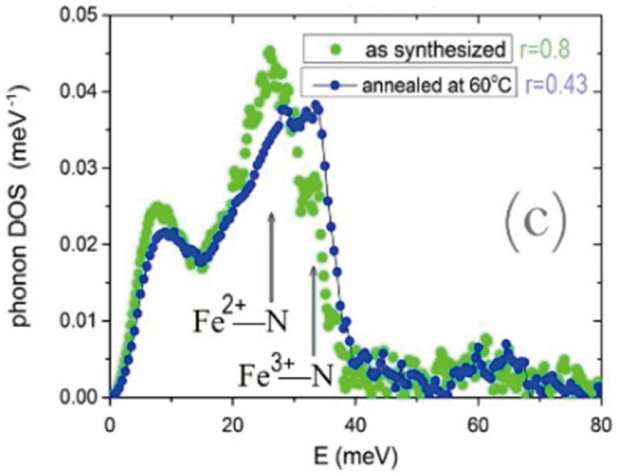

P14

A Contribution of Second Phase into the ^{57}Fe Projected Density of States Peaked Near 20 meV

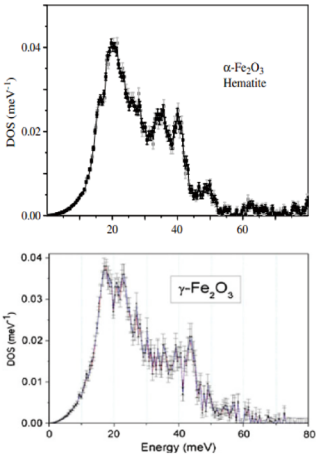

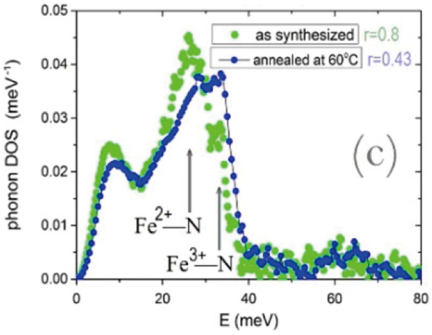

P15

Expectation from

Nuclear Resonant Vibrational Spectroscopy (NRVS)

Also Know as Nuclear Inelastic Scattering (NIS) of Synchrotron Radiation

15

P16

Accelerate the redox cycle of Fe(III) and Fe(II)

Prussian blue/TiO_2 NPs as a heterogeneous photo-Fenton catalyst for degradation of organic pollutants in water

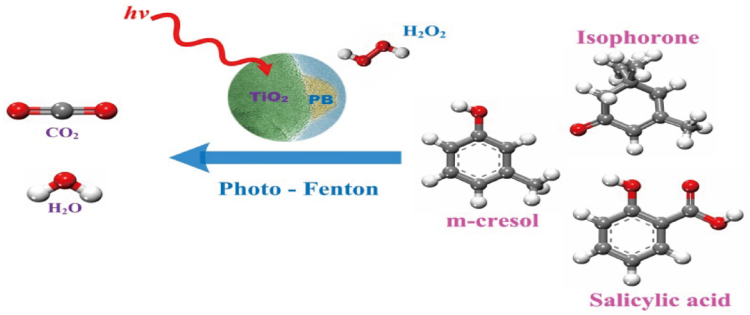

X. Li, J. Wang, et al., Catal. Sci. Technol. 5 (2015) 504.

P17

- **Reaction mechanism and reactive intermediates**

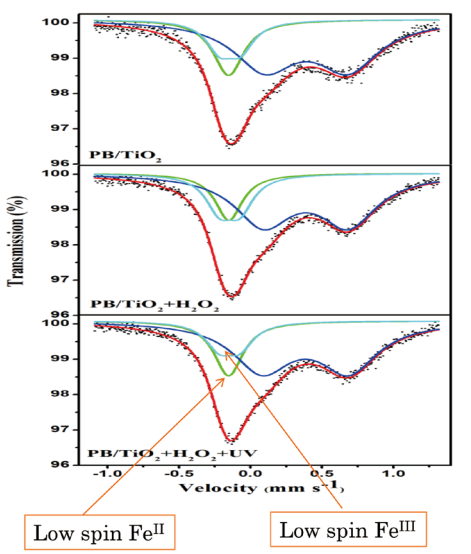

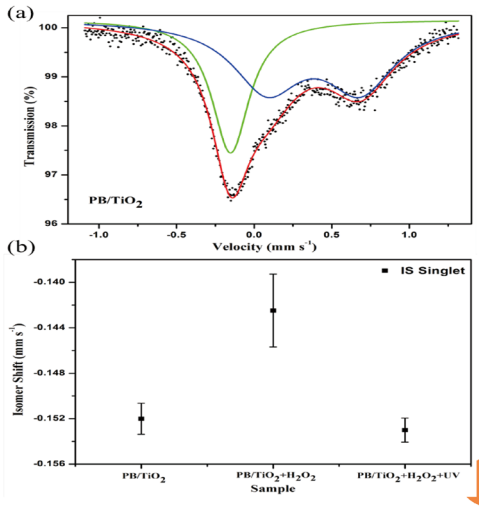

P18

- **Proposed mechanism of PB/TiO_2 as a heterogeneous photo-Fenton catalyst**

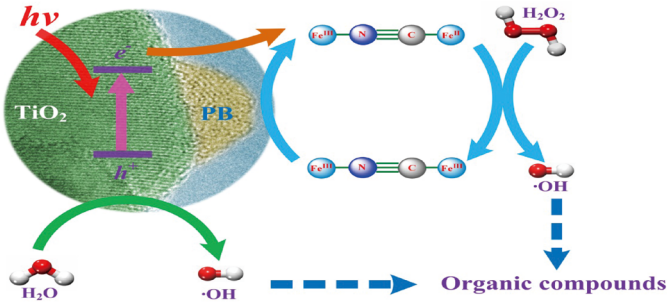

(1) $[Fe^{III}–(NC)_6–Fe^{II}] + H_2O_2 \rightarrow [Fe^{III}–(NC)_6–Fe^{III}] + HO\bullet + OH^-$

(2) $[Fe^{III}–(NC)_6–Fe^{III}] + O^{2-}\bullet \rightarrow [Fe^{III}–(NC)_6–Fe^{II}] + H_2O + 1/2O_2$

(3) $TiO_2 + h\nu \rightarrow e^- + h^+$

(4) $h^+ + H_2O \rightarrow HO\bullet$

(5) $[Fe^{III}–(NC)_6–Fe^{III}] + e^- \rightarrow [Fe^{III}–(NC)_6–Fe^{II}]$

P19

Interfacial Electron Transfer: Iron(III)-bipyridine Complex/TiO_2

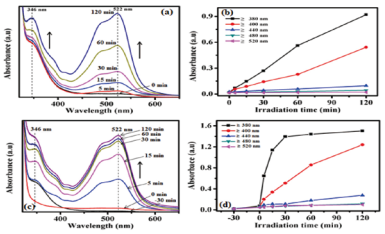

Electronic absorption spectral studies during electron transfer process.

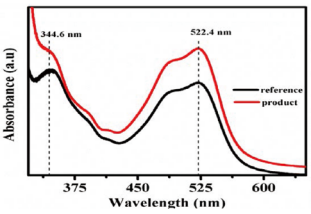

Electronic absorption spectra of solution product and reference complex.

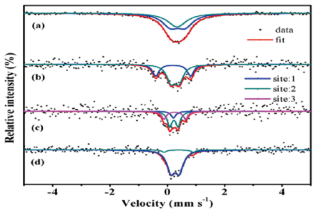

^{57}Fe Mössbauer spectra of solution products (where (a) precursor, (b) reference, (c) product (long wavelength), (d) product (short wavelength)).

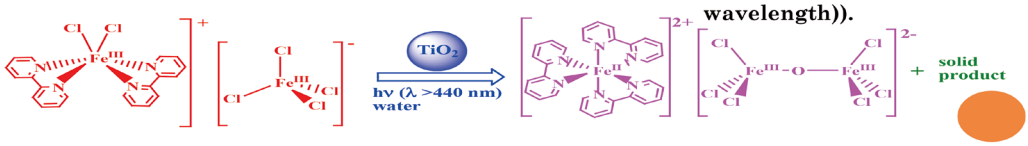

P20

Thank you!